Structure
Article

Structural Basis for Selective Recognition of Endogenous and Microbial Polysaccharides by Macrophage Receptor SIGN-R1

Noella Silva-Martín,[1] Sergio G. Bartual,[1] Erney Ramírez-Aportela,[3] Pablo Chacón,[3] Chae Gyu Park,[2,4,*] and Juan A. Hermoso[1,*]
[1]Department of Crystallography and Structural Biology, Institute of Physical Chemistry "Rocasolano", CSIC, 28006 Madrid, Spain
[2]Laboratory of Cellular Physiology and Immunology and Chris Browne Center for Immunology and Immune Diseases, The Rockefeller University, 1230 York Avenue, New York, NY 10065, USA
[3]Department of Biological Chemical Physics, Institute of Physical Chemistry "Rocasolano", CSIC, 28006 Madrid, Spain
[4]Laboratory of Immunology, Severance Biomedical Science Institute, Brain Korea 21 PLUS Project for Medical Science, Yonsei University College of Medicine, 50-1 Yonsei-ro, Seodaemun-gu, Seoul 120-752, Korea
*Correspondence: chaegyu@yuhs.ac (C.G.P.), xjuan@iqfr.csic.es (J.A.H.)
http://dx.doi.org/10.1016/j.str.2014.09.001

SUMMARY

SIGN-R1 is a principal receptor for microbial polysaccharides uptake and is responsible for C3 fixation via an unusual complement activation pathway on splenic marginal zone macrophages. In these macrophages, SIGN-R1 is also involved in anti-inflammatory activity of intravenous immunoglobulin by direct interaction with sialylated Fcs. The high-resolution crystal structures of SIGN-R1 carbohydrate recognition domain and its complexes with dextran sulfate or sialic acid, and of the sialylated Fc antibody provide insights into SIGN-R1's selective recognition of α-2,6-sialylated glycoproteins. Unexpectedly, an additional binding site has been found in the SIGN-R1 carbohydrate recognition domain, structurally separate from the calcium-dependent carbohydrate-binding site. This secondary binding site could bind repetitive molecular patterns, as observed in microbial polysaccharides, in a calcium-independent manner. These two binding sites may allow SIGN-R1 to simultaneously bind both immune glycoproteins and microbial polysaccharide components, accommodating SIGN-R1's ability to relate the recognition of microbes to the activation of the classical complement pathway.

INTRODUCTION

The classical pathway is one of the major complement activation mechanisms and is required for innate protection against pathogenic microorganisms including *Streptococcus pneumoniae* (Brown et al., 2002). A pivotal step in the complement activation pathway is the assembly of C3 convertase, which digests the complement components to form C3 fragments that bind to microbes and make them recognized by leukocytes. Deposition and activation of C3 convertase over the bacterial surface initiates the complement cascade leading to the elimination of the microbes. However, encapsulated microorganisms like *S. pneumoniae* are able to resist to the complement pathway by limiting access to the cell surface and reducing the amount of C3 deposition (Abeyta et al., 2003). To overcome this problem, hosts have developed an alternative strategy for specific pathogen detection by pattern recognition receptors (PRRs). PRRs discriminate the molecular patterns expressed by pathogens and thus facilitate differential recognition of pathogens and their products by the immune system (Gordon, 2002).

C-type lectin receptors (CLRs) are one kind of PRRs expressed by a broad spectrum of cells, including dendritic cells (DCs), macrophages, and other antigen-presenting cells (Meyer-Wentrup et al., 2005). Increasing evidence has shown that the roles played by several members of the CLR family are critical for innate immunity. SIGN-R1 or CD209b is one of the eight mouse homologs of human CLR named DC-SIGN or CD209 (Park et al., 2001; Powlesland et al., 2006). Unlike human DC-SIGN/CD209, three of mouse SIGN family molecules are found to be expressed in the immune system: DC-SIGN/CD209a, SIGN-R1/CD209b, and SIGN-R3/CD209d. Whereas human DC-SIGN is expressed in both dendritic cells and macrophages (Geijtenbeek et al., 2000; Granelli-Piperno et al., 2005), the expression of three mouse SIGN homologs is detected in different levels from distinct populations of dendritic cells and macrophages (Cheong et al., 2010; Kang et al., 2003; Nagaoka et al., 2010). Of three homologs, mouse DC-SIGN lacks polysaccharide binding, whereas SIGN-R1, similar to human DC-SIGN, binds a broad variety of microbial organisms and their polysaccharides and SIGN-R3 binds a fewer number of ligands (Caminschi et al., 2006; Galustian et al., 2004; Takahara et al., 2004).

SIGN-R1 is expressed at high levels in macrophages within the splenic marginal zone and lymph node medulla and is also a principal receptor for taking up microbial polysaccharides such as dextran or capsular polysaccharides of *S. pneumoniae* (CPSs; Geijtenbeek et al., 2002; Kang et al., 2003, 2004). In vivo inactivation of SIGN-R1 inhibits clearance of *S. pneumoniae* by preventing macrophages from phagocytosis, blocks complement-dependent deposition of CPS on splenic follicles, and therefore makes mice more susceptible to pneumococcal

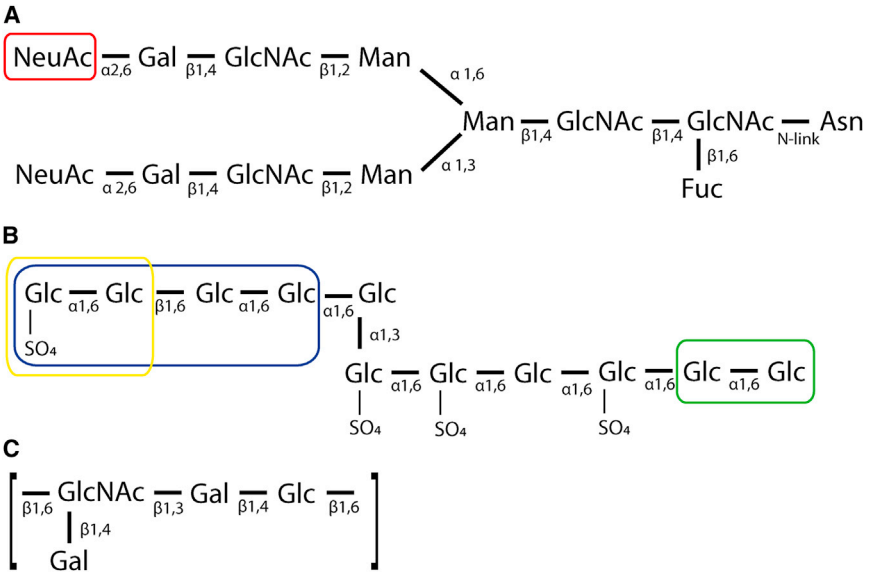

Figure 1. Oligosaccharide Structure

(A) Structure of the full carbohydrate moiety linked to Asn of antibody Fc fragment and subunit A of globular domain of C1q. The sialic acid used in this study is boxed in red.

(B) Structure of the dextran sulfate polysaccharide showing heterogeneous sulfate substitutions. The tetrasaccharide fragment observed in one SIGN-R1 complex is boxed in blue, and two disaccharides also found in complex with SIGN-R1 are boxed in yellow and green.

(C) Repeating unit of capsular polysaccharide belonging to 14 serotype of *S. pneumoniae*. Glc, glucose; Fuc, fucose; Gal, galactose; GlcNAc, N-acetylglucosamine; Man, manose; NeuAc, sialic acid.

infection (Geijtenbeek et al., 2002; Kang et al., 2003, 2004, 2006; Lanoue et al., 2004). This defect in innate immunity against *S. pneumoniae* after inactivation of SIGN-R1 suggests a link between SIGN-R1 and the fixation of C3 opsonins on CPS. This connection was revealed by an unusual complement activation pathway against CPS mediated by SIGN-R1 on splenic marginal zone macrophages (Kang et al., 2006). Binding of CPS to SIGN-R1 initiates an immunoglobulin (Ig)-independent activation of complements for the fixation of C3 on CPS, where the direct interaction between SIGN-R1 and C1q triggers the classical complement pathway. This complement activation strategy in splenic marginal zone macrophages prevents *S. pneumoniae* from escaping C3 opsonization (Kang et al., 2006). In this mechanism, it is critical that SIGN-R1 molecule can function in both processes, i.e., the recognition and binding of a pathogen and the activation of classical complement pathway, which is likely to require SIGN-R1 to bind both CPS and C1q simultaneously. In addition, it has been reported that SIGN-R1 clears out the cells via interaction with C1q fixed on apoptotic cells, thus increasing the C3 fixation (i.e., complement activation) on the apoptotic cells, and reducing autoimmunity (Prabagar et al., 2013).

The cause of anti-inflammatory activity of intravenous Ig (IVIG) was contributed to a minor population of the pooled IgG molecules that contains terminal α-2,6-sialic acid linkages on their Fc-linked glycans (Kaneko et al., 2006). It was reported that SIGN-R1 in splenic marginal zone macrophages preferentially binds to the sialylated Fcs and that the in vivo inactivation of SIGN-R1 eliminates the anti-inflammatory activity of IVIG and intravenous sialylated Fcs (Anthony et al., 2008). This interaction between SIGN-R1 and sialylated Fcs was shown to accomplish the anti-inflammatory activity via a different Th2 cytokine pathway (Anthony et al., 2011). Therefore, SIGN-R1 is a single member of the mouse SIGN CLR family that functions by binding polysaccharides from both endogenous and microbial origins.

We report herein the high-resolution crystal structures of the carbohydrate recognition domain of SIGN-R1 (CRD_SIGN-R1) as well as their complexes with dextran sulfate (DexS) and sialic acid (N-acetylneuraminic acid [NeuAc]; Figure 1). In addition, the high-resolution crystal structure of the sialylated Fc antibody portion obtained in this work together with molecular dynamics calculations, provides insights into SIGN-R1's selective recognition of α-2,6-sialylated glycoproteins relevant to the role of SIGN-R1 in anti-inflammatory activity of IVIG. Structural, computational and biochemical experiments reveal that sialylated glycoproteins, such as C1q and Ig, bind SIGN-R1 through the classical calcium-dependent carbohydrate recognition site, whereas the binding of microbial pathogens can also use the additional calcium-independent substrate-binding site, thereby allowing SIGN-R1 to simultaneously bind both immune glycoproteins and microbial components.

RESULTS AND DISCUSSION

Overall CRD_SIGN-R1 Structure

With the extracellular domain of SIGN-R1 (ECD_SIGN-R1) produced as monomers from *Escherichia coli*, crystals could not be generated (P. Li, personal communication). In addition, with the ECD_SIGN-R1 produced as His-tagged monomers in *E. coli*, carbohydrate binding could not be detected even after oligomerization with anti-His antibody (T. Feizi, personal communication). Powlesland and colleagues also reported that the ECD_SIGN-R1 produced from *E. coli* was unable to bind any carbohydrates as monomers (Powlesland et al., 2006). Therefore, it is likely that the ECD_SIGN-R1 or CRD_SIGN-R1 proteins prepared from *E. coli* are not properly folded. Previously, however, we had successfully performed the carbohydrate binding analyses of SIGN-R1, where the soluble Fc-fused ECD_SIGN-R1 was expressed and purified directly from the culture supernatant of transfectant Chinese hamster ovary (CHO) cells (Galustian et al., 2004). Therefore, we prepared the soluble CRD_SIGN-R1 (amino acid residues from Cys192 to Gly325) from the culture supernatant of transfectant CHO cells and made its crystals successfully (Silva-Martin et al., 2009).

High-resolution crystal structures for CRD_SIGN-R1 and its complexes with dextran sulfate (SIGN-R1:DexS) and sialic acid (SIGN-R1:NeuAc) have been solved in this study (Table 1). The asymmetric unit is composed of four nearly identical monomers with an average root-mean-square deviation (rmsd)

Table 1. Data Collection and Refinement Statistics

	CRD-SIGN-R1	CRD-SIGN-R1:DexS	CRD-SIGN-R1:NeuAc	FC_Sial
Data Collection				
Space group	C2	C2	C2	$P2_12_12_1$
Cell dimensions				
a, *b*, *c* (Å)	146.72, 92.77, 77.06	144.03, 97.96, 73.84	146.20, 94.47, 76.14	49.59, 80.15, 140.21
α, β, γ (°)	90, 121.66, 90	90, 120.86, 90	90, 121.42, 90	90, 90, 90
Temperature (K)	100	100	100	100
Wavelength (Å)	1.07225	0.9334	0.87260	0.999
Resolution (Å)	74.53–(1.98–1.87)	61.815–(2.98–2.58)	42.98–(2.95–2.80)	42.17–(2.42–2.30)
No. unique reflections	52,474 (2,478)	30,140 (2,478)	21,870 (3,185)	25,633 (3,662)
R_{sym} [a]	0.06 (0.54)	0.11 (0.28)	0.11 (0.45)	0.09 (0.51)
Average $I/\sigma(I)$	11.80 (1.70)	6.2 (1.8)	9.4 (3.7)	11.7 (3.5)
Completeness (%)	93 (72)	99 (99)	100 (100)	99.9 (100)
Redundancy	5.7 (5.4)	4.4 (2.4)	2.3 (2.3)	6.4 (6.6)
Refinement				
Resolution (Å)	27.63–1.87	40.00–2.6	40.31–2.80	20.10–2.03
R/R_{free} (%)	20.45/24.43	20.05/24.74	18.06/26.21	23.64/28.21
No. atoms				
Protein	4,292	4,315	4,295	3,316
Water	407	168	479	82
Ligand	–	147	63	221
Metal ions (Ca)	4	4	4	–
SO_4	24	12	30	–
B-factor (Å^2)				
Protein	34.29	30.74	26.55	42.82
Ligands	–	63.45	59.69	61.15
Water	24.88	23.70	24.67	37.63
Rmsds				
Bond length (Å)	0.012	0.011	0.018	0.011
Bond angles (°)	1.063	1.257	1.141	1.257
PDB code	3ZHG	4C9F	4CAJ	4CDH

Value for the highest resolution shell is shown in parentheses.
[a] $Rsym = \Sigma| I - Iav |/ \Sigma I$, where the summation is over symmetry equivalent reflections.

value of 0.182 Å over 126 aligned Cα atoms. The CRD_SIGN-R1 structure (Figure 2A) exhibits one large β strand (β2), which divides the framework in two lobes. The upper lobe comprises β strands 2 to 4 and the α3 helix. The lectin characteristic long loop region (LLR) involved in calcium-mediated carbohydrate binding is found between α3 and β3 (Tyr280 to Asp293; Figure 1). The lower lobe includes the N-terminal and the C-terminal extremes, coming close together to form an antiparallel β sheet that is flanked by α1 and α2, one on each side. Eight cysteines are involved in the formation of four disulfide bridges, three of them stabilizing the lower lobe, while the fourth is located between both lobes. The "WMGL" motif present in all C-type lectin proteins reported (Zelensky and Gready, 2003) is also present in SIGN-R1 (residues 253–256). This pattern unites a cluster of hydrophobic residues stabilizing all parts of the structure. The human C-type lectin DC-SIGN (Protein Data Bank [PDB] code 2IT6) is the most closely related structure to SIGN-R1, with 69% of sequence identity and an rmsd of 1.32 Å over 131 aligned C-alpha atoms.

SIGN-R1 presents six sulfate molecules bound to each monomer (Figure 2A); S1 is near the calcium$^+$-mediated carbohydrate binding site, S6 is placed in the lower lobe near the N-terminal and the C-terminal extremes, and four sulfate molecules (S2–S5) are placed at the opposite face of the calcium-mediated carbohydrate binding site (Figure 2A). Interestingly these four sulfates are located inside a positively charged groove in collar pattern disposition, retaining a similar distance among them (8.70 Å, 9.94 Å, and 8.46 Å; Figure 2B).

Calcium-Binding Site in SIGN-R1

In general, altogether, four Ca^{2+}-binding sites occur in different subgroups of the C-type lectin-like domain (CTLD) family (Zelensky and Gready, 2003). In the crystal structure of SIGN-R1 only one, that of the characteristic C-type lectin sugar-binding site, is observed (Figure 2A). This Ca^{2+} is stabilized by carboxylate or carboxyamide groups of Glu285, Asn287, Glu292, and Asp304 and by two water molecules, providing an octahedral coordination for the cation (Figure S1A available online). All these

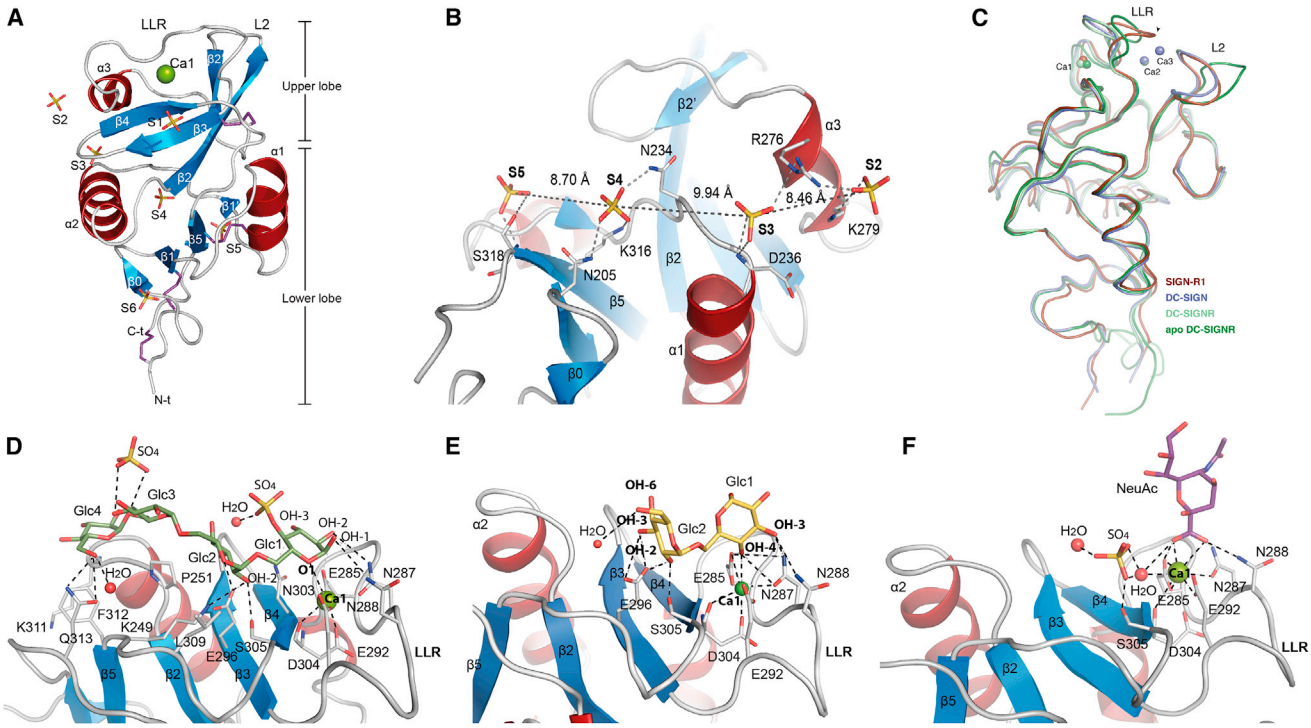

Figure 2. 3D Structure of CRD_SIGN-R1

(A) Overall view of the ribbon representation of CRD_SIGN-R1. The Ca^{2+} ion (Ca1) is represented as a green sphere, and the six bound sulfate molecules (S1–S6) are drawn as capped sticks. Disulfide bridges are shown as purple sticks.

(B) Stabilization of four sulfate molecules (S2–S5) placed at the opposite face of the primary carbohydrate binding site. Residues involved in sulfate stabilization are labeled and represented as capped sticks. Polar interactions are represented as dotted lines and distances among sulfates are also indicated.

(C) Structural superimposition of SIGN-R1 (brown), DC-SIGN (blue), DC-SIGNR (light green), and the apo form of DC-SIGNR (dark green). The three Ca^{2+} ions found in these CTLD structures altogether are shown as spheres.

(D) DexS tetrasaccharide in complex with SIGN-R1.

(E) Dex disaccharide in complex with SIGN-R1.

(F) Sialic acid in complex with SIGN-R1. Relevant residues are drawn as capped sticks and labeled for SIGN-R1.

residues are part of two characteristic motifs present in most of the CTLD superfamily sequences: the "EPN" motif (residues 285–287) that belongs to the LLR and the "WND" motif (residues 302–304) from the β4 strand (Figure S1C). Interestingly, the Asn303 in SIGN-R1, which is part of the "WND" motif, is not coordinating the calcium ion (Figure S1A) as occurs in the other known structures of sugar-binding C-type lectins either alone or in complex with a ligand (Figure S1B). Structural analysis also reveals that the LLR region from SIGN-R1 presents a different conformation among all reported CTLD members (Figure 2C). The cavity in which secondary calcium ions (i.e., Ca2 and Ca3) are located in human DC-SIGN is occupied by the LLR loop in SIGN-R1, therefore avoiding interaction with these two calcium atoms (Figure S1D). The L2 loop has been observed in two different conformations (closed and open) in DC-SIGNR, depending on the presence or absence of the secondary calcium ions. In SIGN-R1, the L2 loop is folded in the closed conformation (Figure 2C) without the presence of secondary Ca ions. Two residues, Ile289 from LLR and Ala263 from L2 (neither present in DC-SIGN nor in DC-SIGNR), stack with hydrophobic residues of the cavity masking the secondary calcium-binding cavity (Figure S1D). The presence of a salt bridge interaction between Glu291 and Lys306 further stabilizes the conformation of the LLR loop (Figure S1D). It is worth mentioning that crystallization with an excess of Ca^{2+} did not result in any modification of the 3D structures of SIGN-R1 either in the native or in the complexes with substrates. Mechanistic implications of these differences in residues and loop conformations in SIGN-R1 and DC-SIGN/DC-SIGNR cannot be overstated. Mutagenesis experiments on residues in DC-SIGN (Val351) and in DC-SIGNR (Ser363), equivalent to Ile289 of SIGN-R1, revealed that they are the main responsible residues for binding specificity of DC-SIGN to fucose and DC-SIGN-R to mannose, respectively (Guo et al., 2004).

Carbohydrate Recognition through Canonical Site

Carbohydrates that bind to SIGN-R1 have been previously explored with glycan-array tests, suggesting the specificity of SIGN-R1 for mannose, fucose, and DexS, among other polysaccharides (Galustian et al., 2004). Besides, SIGN-R1 has been reported to bind sialic acid present on antibodies or glycoproteins such as C1q complement factor (Anthony et al., 2008; Mizuochi et al., 1978).

In the SIGN-R1:DexS complex, three of the four monomers of the asymmetric unit presented electron density for DexS moieties (one tetrasaccharide unit and two disaccharide units

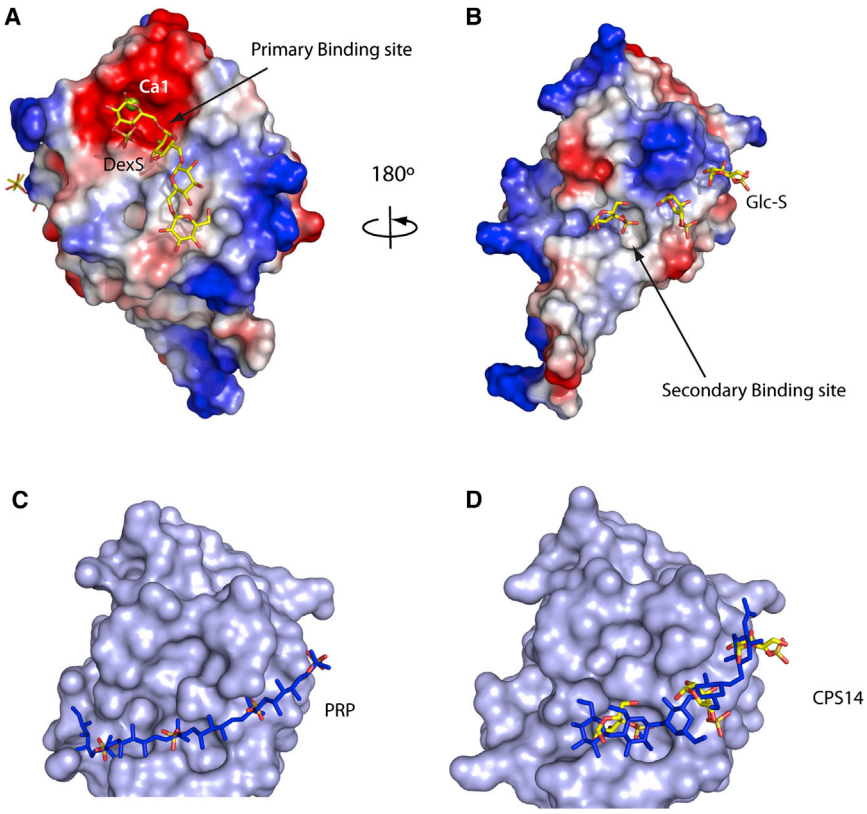

Figure 3. Primary and Secondary Binding Sites in SIGN-R1

(A) DexS tetrasaccharide interacting with SIGN-R1 primary binding site. Electrostatic potential on SIGN-R1 molecular surface is represented with acidic regions in red and basic regions in blue.

(B) DexS moities (Glc-S) interacting with SIGN-R1 secondary binding site.

(C) Model of polyribitol phosphate (blue sticks) docked over the SIGN-R1 secondary binding site. Sulfate molecules (yellow sticks) observed in the crystal structure of SIGN-R1 are superimposed for comparison.

(D) Model of CPS14 (blue sticks) docked over SIGN-R1 secondary binding site. Glc-S molecules (yellow sticks) as observed in the SIGN-R1:DexS complex are superimposed for comparison.

respectively, see Figure 1B) in the Ca^{2+}-mediated primary binding site of the lectin (Figures 2D and 2E; Figure S2). The Ca^{2+}-mediated interactions with dextran depend on the presence or absence of a sulfate molecule attached to the glucose sugar. When the sugar contains a sulfate molecule (as occurs in the tetrasaccharide and one of the disaccharides; Figure 2D), the sugar ring interacts with calcium through the O1 and establishes hydrogen bonds between its OH-1 with Asn287 and Asn288, the OH-2 with Glu285, and the OH-3 with Asn303. When the sugar does not possess this sulfate moiety, interaction with Ca^{2+} is made through the OH-4, whereas OH-3 interacts with residues Asn287 and Asn288 (Figure 2E). It is worth noting that due to SIGN-R1's conformation of LLR, Asn288 plays a key role in carbohydrate binding but not in binding of one of the secondary Ca^{2+} as occurs in human DC-SIGN(R). Protein interactions with the second sugar ring are conserved in all three DexS complexes (Figures 2D and 2E). The tetrasaccharide extends its binding through rings three and four by hydrophobic interactions with Pro251 and Phe312. The fourth ring also establishes hydrogen bonds with Gln213 (Figure 2D).

In the crystal structure of the SIGN-R1:NeuAc complex, all four monomers of the asymmetric unit present the sialic acid attached (Figures 2F and S2). The carboxylic group of the sialic acid replaces the interaction of the two water molecules of native SIGN-R1 in the octahedral coordination of the calcium ion. Sialic acid is strongly stabilized by SIGN-R1 because most of residues involved in calcium binding (Glu285, Asn287, Glu292) also interact with sialic acid, yielding a large hydrogen bond interaction network (Figure 2F). Interestingly, as also observed in SIGN-R1:DexS complexes, the Asn288 contributes to this network interaction in SIGN-R1.

A Secondary Binding Site in SIGN-R1

Analysis of the density maps of SIGN-R1:DexS complex revealed the presence of three well-defined molecules of D-glucose-4-sulfate (Glc-S) at the opposite face of the canonical binding site (Figure 3B). This secondary site is a 30-Å long basic groove that is formed by loops connecting α1 and α2, α3 and β2′, and by the lower lobe β sheet. Glc-S molecules occupy the positions of the sulfate molecules S3–S5 found in the native structure (Figure 2). Remarkably, both the sulfate moiety and the glycan part of Glc-S are well stabilized in the SIGN-R1:DexS complex (Figures 3B and S2E).

The repetitive disposition of sulfate/sugar molecules recognized by SIGN-R1 through this secondary binding site pushed us to explore SIGN-R1 binding to other cellular components sharing a similar repetitive structure. Teichoic acids (TAs), one of the main components of the cell wall of all gram-positive bacteria, are formed by repeating units of sugar-phosphate chains (Weidenmaier and Peschel, 2008). These glycopolymers are frequently formed by glycerol or ribitol groups linked by phosphodiester bridges as in TAs from *Staphylococcus aureus* or *Listeria monocytogenes* (Weidenmaier and Peschel, 2008). Docking calculations reveal that polyribitol phosphate chain of TAs nicely fits into SIGN-R1's secondary binding site with phosphate moieties superimposing onto the S3–S5 molecules found in SIGN-R1 (Figure 3C). Another repetitive structure is that of capsular pneumococcal polysaccharide 14 (CPS14; Figure 1). It has been found that SIGN-R1 binds preferentially to this capsular polysaccharide (Kang et al., 2004). Docking calculations also show binding of CPS14 to this region of SIGN-R1 (Figure 3D). Docked sugar rings replace the crystallographic glucose molecules found in the SIGN-R1:DexS complex.

The additional secondary binding site in SIGN-R1 is calcium independent and structurally not related to the canonical

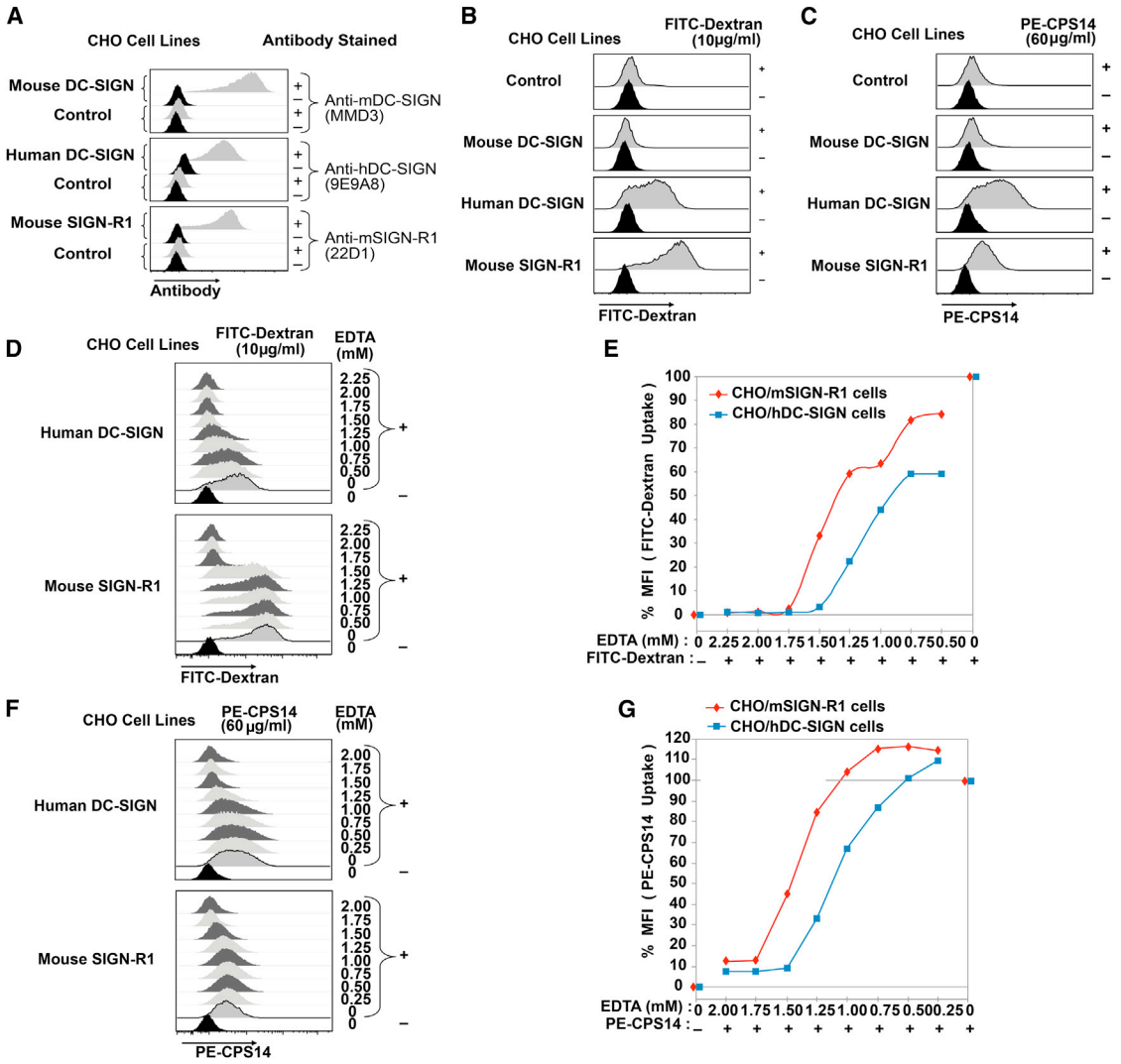

Figure 4. Binding of Polysaccharides to SIGN-R1 Is Less Sensitive to EDTA Than Human DC-SIGN

(A) CHO cells expressing neomycin (CHO/control), mouse DC-SIGN (CHO/mDC-SIGN), mouse SIGN-R1 (CHO/mSIGN-R1), and human DC-SIGN (CHO/hDC-SIGN) are stained with(+)/without(−) specific antibodies as indicated at the right side.

(B) Each CHO cell was incubated with(+)/without(−) FITC-dextran (500 kDa, 10 μg/ml) for 1 hr followed by fluorescence-activated cell sorting (FACS) analysis.

(C) Each CHO cell was incubated with(+)/without(−) PE-CPS14 (60 μg/ml) for 5 hr followed by FACS analysis.

(D) Each CHO cell was incubated with(+)/without(−) FITC-dextran (10 μg/ml) and EDTA (0 to 2.25 mM) for 1 hr followed by FACS analysis.

(E) Percent values for mean fluorescence index (MFI) of each flow cytogram in (D) were plotted, where 100% is for FITC-dextran incubated without EDTA and 0% for no FITC-dextran.

(F) Each CHO cell was incubated with(+)/without(−) PE-CPS14 (60 μg/ml) and EDTA (0–2.00 mM) for 5 hr followed by FACS analysis.

(G) Percent values for MFI of each flow cytogram in (F) were plotted, where 100% is for PE-CPS14 incubated without EDTA and 0% for no PE-CPS14. Data in (D)–(G) represent one of three independent experiments showing similar results, respectively.

binding site. Whereas the binding of SIGN-R1 to microbial polysaccharides is calcium dependent (Galustian et al., 2004; Nagaoka et al., 2005; Takahara et al., 2004); i.e., EDTA at 5 mM or higher concentration prevents SIGN-R1 from binding to its polysaccharide ligands. This implies that, although the primary and secondary binding sites are spatially separate, polysaccharides might use both sites to bind SIGN-R1. In agreement with this, it has been reported that SIGN-R1 can only bind to dextrans with high molecular weights but other SIGNs can bind to dextrans with high as well as lower molecular weights (Takahara et al., 2004). To test this model, we compared the polysaccharide-binding activities of SIGN-R1 with those of human DC-SIGN (hDC-SIGN), which lacks a calcium-independent secondary binding site. In both cases of FITC-labeled dextran (500 kDa) and PE-labeled CPS14, the CHO cells expressing SIGN-R1 were able to bind these polysaccharides at 0.25–0.5 mM higher concentration of EDTA than the CHO cells expressing hDC-SIGN (Figure 4). This may indicate that SIGN-R1 contains an extra calcium-independent binding site for dextran and CPS14, making

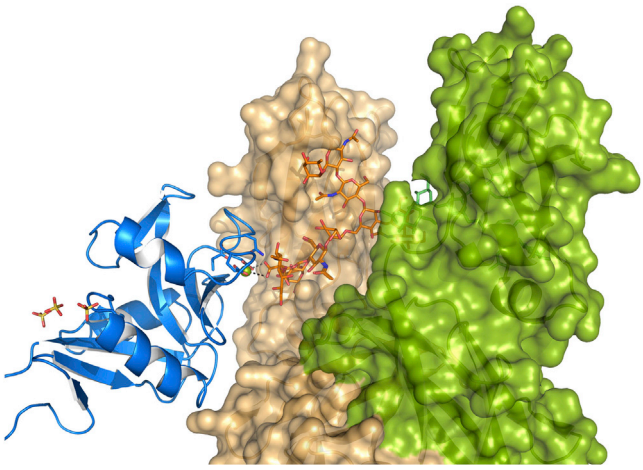

Figure 5. Model of Interaction between SIGN-R1 and α-2,6 Sialylated Antibody

Superimposition of the crystal structure of SIGN-R1:NeuAc (blue ribbon) with the crystal structure of α-2,6 sialylated antibody (molecular surface in brown for chain A and in green for chain B). Canonical binding site of SIGN-R1 is represented with the Ca ion (green sphere) and residues coordinating it (blue capped sticks). The LLR loop is labeled. The secondary binding site of SIGN-R1 is located at the opposite face where sulfate molecules (represented as capped sticks) are found. Oligosaccharides attached to Fc are represented as orange-capped sticks. The terminal α-2,6 sialic acid was not visible in the crystal structure; the coordinates for this terminal sugar have been taken from the energy-minimized model. SIGN-R1:Fc interaction mediated by sialic acid carboxylate would be the starting anchor for further interaction with other sugars from the carbohydrate moiety linked to Fc. A complementarity exists between the protein surfaces of the SIGN-R1 receptor and the antibody, pointing to a protein-protein interaction upon glycan recognition.

their binding less sensitive to EDTA treatment, compared to hDC-SIGN.

Implications in Anti-inflammatory Activity of Intravenous Ig

SIGN-R1 plays an essential role in the anti-inflammatory process induced by IVIG (Anthony et al., 2008). In this process, SIGN-R1 specifically recognizes α-2,6 sialylated antibodies instead of α-2,3 sialylated antibodies. According to our study on the SIGN-R1:NeuAc complex, SIGN-R1 interacts with sialic acid through the carboxylate moiety. The atomic resolution of an α-2,3 sialylated antibody (PDB code 1MCO; Guddat et al., 1993) shows the carboxylic group of sialic acid occluded and facing the inner part of the antibody, therefore it is not able to interact with SIGN-R1 as found in the SIGN-R1:NeuAc complex.

To shed more light on the interaction between SIGN-R1 and silalylated Fc, we solved the high-resolution structure of a human α-2,6 sialylated antibody Fc portion by X-ray crystallography (Table 1; Figure S3A). The density maps of the α-2,6 Fc structure were of excellent quality and allow us to trace almost the complete glycan chain but without the terminal sialic acid that was not visible in our maps (Figure S3B), indicating a high flexibility of this terminal sugar. The crystal structure of an α-2,6 sialylated antibody has been reported (PDB code 4BYH; Crispin et al., 2013). Despite completely different crystallization conditions, our α-2,6 Fc structure was nearly identical to the reported α-2,6 sialylated antibody in both the backbone (rmsd of 0.563 Å over 294 aligned Cα atoms) and the sugar conformation (Figures S3C and S3D). Interestingly, the α-2,6 Fc structure shows the carboxylic group of arm 6 terminal sialic acid as completely exposed (Figures S3D and S3E), allowing the interaction with SIGN-R1 as observed in the SIGN-R1:NeuAc complex.

Molecular dynamic (MD) simulations further indicate that α-2,3 and α-2,6 sialylations result in two different conformers for the sialic acid. In α-2,3 sialylated antibody both galactose and sialic acid rings establish strong interactions with the protein (Figures S4 and S5; Movie S1), provoking the carboxylate moiety being occluded (accessible surface of 0.3 $Å^2$). In the α-2,6 sialylated antibody, the galactose interacts with the protein while the sialic acid is completely exposed (accessible surface of 5 $Å^2$), releasing some regions of Fc antibody (Figures S5 and S6; Movie S2). This high flexibility is in agreement with what we observe in our crystal structures.

Summing up, whereas the α-2,6 link provokes exposition of carboxylic acid of the sialic acid, the α-2,3 variant does not. Therefore only the α-2,6 link could allow Fc recognition by SIGN-R1. Superimposition of both SIGN-R1 and Fc structural models (Figure 5) indicates that their interaction mediated by sialic acid carboxylate would be the starting anchor for further interaction with other sugars from the carbohydrate moiety linked to Fc (as observed in the DexS tetrasaccharide in complex with SIGN-R1) and to allow interaction between both protein surfaces (specially through the LLR loop from SIGN-R1 and with the exposed Fc region in the α-2,6 variant predicted with MD). It has been proposed that structural changes in Fc upon sialylation would be responsible for the interaction with the receptor (Sondermann et al., 2013a) and that the high-salt crystal structure of the α-2,6 sialylated antibody reported previously (Crispin et al., 2013) would not be representative of the conformational changes found in solution (Sondermann et al., 2013b). Considering that we have obtained a nearly identical structure for α-2,6 sialylated antibody in the absence of salt, it is expected that changes in the Fc should be more related with those predicted by our MD simulations. These results would provide an structural explanation for the observed specificity of SIGN-R1 to α-2,6 sialylated antibodies in the inhibition of the inflammatory response (Anthony and Ravetch, 2010).

Complement Fixation Pathway for Pathogens Initiated by SIGN-R1

SIGN-R1 presents a single calcium-binding site that corresponds to the primary carbohydrate-binding site observed in other CTLDs. The specific conformation of SIGN-R1 for the LLR loop avoids stabilization of Ca2 and Ca3.

Crystal structures of SIGN-R1 alone and in complex with DexS reveal the presence of sulfate or Glc-S moieties, respectively, both of which are attached to SIGN-R1's calcium-independent secondary binding site in a repetitive manner. This additional binding site is located at the opposite face of the canonical calcium-dependent binding site without apparent structural connection among them. Docking calculations indicate that polyribitol phosphate (backbone of teichoic acids of some microbial pathogens), which follows the same repetitive pattern, can be accommodated in this secondary binding site. The same result is also observed for docking with a model of the capsular

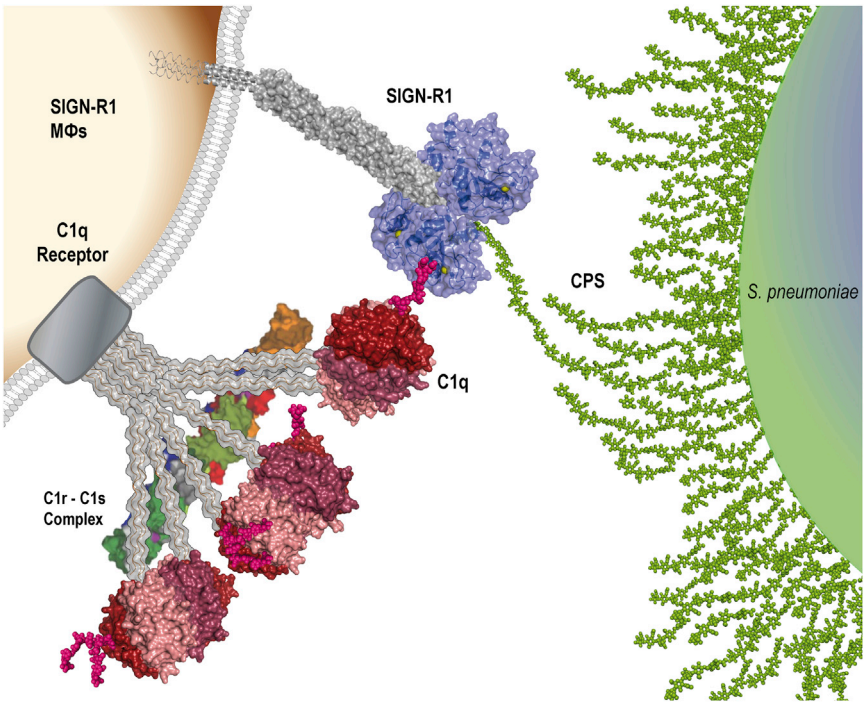

Figure 6. Proposed Mechanism of Pathogen Recognition and Complement Activation Mediated by SIGN-R1

Molecular surface of SIGN-R1 crystal structure is shown in blue with Ca^{2+} atoms drawn as yellow spheres. A model for the extracellular SIGN-R1 tetramer attached to the macrophage membrane is presented. The carbohydrate recognition domain of SIGN-R1 can recognize pathogen components such as CSP through its secondary binding site that binds the globular portion of C1q (PDB code 1PK6; Gaboriaud et al., 2003) through the calcium-dependent binding site.

polysaccharides from pneumococcus serotype 14 (CSP14). Altogether, these results indicate that SIGN-R1 possesses two separate binding sites. The additional noncanonical binding site in SIGN-R1 might recognize distinct carbohydrate patterns from microbial pathogens, such as dextran, teichoic acids, and CPS14.

SIGN-R1 mediates activation of the classical complement pathway through direct interaction with C1q and CPS in spleen (Kang et al., 2006). How exactly these molecules interact to activate the complement pathway is unknown. C1q is a glycoprotein and the structure of its recognition domain (Gaboriaud et al., 2003) and sugar chains has been reported (Mizuochi et al., 1978). Structures of oligosaccharides attached to C1q are represented in Figure 1A (or small variants with only one NeuAc at the end or without the Fuc at the beginning of the chain). In all cases, the sialic acid is exclusively linked at the C-6 position of the galactose residue. Furthermore, it has been reported that SIGN-R1 specifically recognizes IgG molecules that contain terminal α-2,6 sialic acid linkages (Anthony et al., 2008). The crystal structure of the SIGN-R1:NeuAc complex reveals that sialic acid is strongly stabilized by SIGN-R1 at the primary canonical carbohydrate binding site (but not in the secondary site) through carboxylic acid in NeuAc. Considering all these facts, we propose a model that the SIGN-R1 lectin captures C1q, which is bound to C1r and C1s in serum, via a direct interaction between the primary carbohydrate binding site in SIGN-R1 and the polysaccharides ended by an α-2,6 sialic acid in C1q, whereas SIGN-R1 also binds to pathogen patterns through its secondary binding site (Figure 6).

However, seeing that the binding of microbial polysaccharides to SIGN-R1 expressed on cell lines is less but still sensitive to EDTA treatment (Figure 4), this model for simultaneous recognition of two different polysaccharides by SIGN-R1 (Figure 6) may not explain all the binding events mediated by SIGN-R1 on splenic marginal zone macrophages. SIGN-R1 protein in spleen and lymph nodes and expressed in cell lines exists in highly complex forms that have much higher molecular weights than tetrameric forms (Kang et al., 2003). In addition, cell lines expressing SIGN-R1 cannot bind $\leq$ 40 kDa dextrans, whereas other CLRs such as SIGN-R3 and Langerin can bind 40 kDa of dextran (Takahara et al., 2004). Based on these observations, we propose that on the surface of splenic marginal zone macrophages, where SIGN-R1 is expressed as large complexes of multiple tetramers, microbial polysaccharides such as dextran and CPS14 bind to SIGN-R1 on both of its calcium-dependent and -independent sites. Meanwhile, Ca-dependent primary binding sites in a significant number of SIGN-R1 molecules in the same complexes might bind to the terminal α-2,6 sialic acid of polysaccharides in C1q (Figure 6). Therefore, the interaction with two different polysaccharides would allow SIGN-R1 complexes to efficiently identify and bring the microbial pathogen to the proximity of C1q, thus promoting the assembly of a C4bC2a, i.e., C3 convertase, and the C3 fixation of microbial polysaccharides. This mechanism could allow the efficient activation and fixation of C3 by *S. pneumoniae* and CPS upon entry into the bloodstream and spleen. Then, within minutes of intravenous injection, both CPS and *S. pneumoniae* are fixed with C3 to be sequestered from marginal zones to follicles, and much of the C3 in serum is catabolized (Kang et al., 2006).

Recent evidence suggests that complement and cellular complement receptors also play important roles in the localization and retention of nonbacterial pathogens to follicular dendritic cells, especially HIV-1 (Feinberg et al., 2007). Interestingly SIGN-R1 binds viral glycoproteins as do human DC-SIGN(R) (Curtis et al., 1992). DC-SIGN binding to HIV can promote viral infection of T cells (Chehimi et al., 2003). It is worth noting that oligosaccharides present on the envelope of various viruses such as HIV also contain terminal α-2,6 sialic acid linkages (Varchetta et al., 2013). Therefore, in the mechanism we proposed, viral glycoproteins could block the interaction of sialylated C1q or Ig with SIGN-R1 through its primary binding site, thus avoiding efficient recognition and response against the pathogen by the immune system.

EXPERIMENTAL PROCEDURES

Production of SIGN-R1

A DNA construct encoding the soluble CRD protein of SIGN-R1 (CRD_SIGN-R1) was generated by amplifying the CRD domain from SIGN-R1 cDNA by PCR, cloned into a mammalian expression vector containing signal sequence and FLAG epitope and sequenced, as described previously (Park et al., 2008). The mammalian expression vector encoding this FLAG-tagged CRD_SIGN-R1 (GenBank accession number EU697459) was transfected into Chinese hamster ovary (CHO) cells (CHO-S cells, GIBCO, Life Technologies) using Lipofectamine 2000 reagent (Life Technologies) following the manufacturer's instructions. Stable CHO cell lines producing the soluble or mature form of FLAG-tagged CRD_SIGN-R1 protein that consists of an N-terminal, 9 amino acid long FLAG epitope and a 134 amino acid long CRD domain of SIGN-R1 (residues from Cys192 to Gly325) were generated following selection with G418 (1.5 mg/ml) as described previously (Kang et al., 2004). CRD_SIGN-R1 protein was purified from the supernatant of stably transfected CHO cell culture with an affinity column using anti-FLAG M1 agarose gel (Sigma-Aldrich) following the manufacturer's instructions.

Binding Experiments

The cDNA encoding an open reading frame of human DC-SIGN (hDC-SIGN) was cloned by PCR from a human thymic cDNA library (Clontech). CHO cells expressing hDC-SIGN were generated and cloned under G418 (1.5 mg/ml) selection pressure as described above. Stable FITC-labeled dextran (FITC-dextran, 500 kDa) was purchased from Sigma-Aldrich. PE-labeled CPS14 (PE-CPS14) was generated at home as follows. Purified CPS14 (lyophilized pneumococcal polysaccharide powder type 14) was purchased from ATCC, and 2 mg of CPS14 was biotinylated in essence as described previously (Colino and Snapper, 2007; Koesling et al., 2001). After extensive dialysis against Dulbecco's PBS (GIBCO, Life Technologies), 500 μg of biotinylated CPS14 in DPBS was mixed with 25 μg of PE-conjugated streptavidin (BD Biosciences) by rotator at 4°C overnight. CHO cells expressing SIGN-R1 (Kang et al., 2004) and hDC-SIGN (see above) were trypsinized and plated into 12-well plates. When the plated CHO cells became confluent, each well was replenished with fresh media containing FITC-dextran (10 μg/ml in final concentration) or PE-CPS14 (60 μg/ml in final concentration) with/without graded doses of EDTA. Then the plates were further incubated at 5% CO_2, 37°C for 1 hr (FITC-dextran) or 5 hr (PE-CPS14) before being analyzed for polysaccharide uptake with a LSR II flow cytometer (BD Biosciences).

Production of α-2,6 Sialylated Antibody

Hypersialylated human Fcs were generated as previously described, with minor modifications (Anthony et al., 2008). Briefly, IVIG-derived Fc fragments were treated with 2,3/6 sialidase to remove sialic acid residues. Fc fragments (30 mg/ml) were incubated in 50 mM MOPS, pH 7.2, 20 mM $MnCl_2$ with 10 μM uridine diphosphate-galactose and 25 mU/10mg substrate of β1-4 galactosyltransferase for 48 hr at 37°C. Next, the Fcs were sialylated in 50 mM MOPS, 20 mM $MnCl_2$, pH 7.2, and 10 mM $MnCl_2$, supplemented with 10 μM CMP-sialic acid, 100 mU/ml α2-6 sialyltransferase at 37°C for 48 hr. The glycosylation reactions were confirmed by lectin blotting with Erythrina Cristagalli Lectin (terminal galactose), and Sambucus Nigra Lectin (terminal 2,6 sialic acid).

Crystallization of SIGN-R1 and SIGN-R1 Complexes

Crystallization trials were performed at 18°C as previously described (Silva-Martin et al., 2009). Good quality crystals grown by mixing 1 μl of CRD_SIGN-R1 (4 mg/ml in 20 mM Tris/HCl pH 7.5 and 100 mM NaCl) with 1 μl of precipitant solution from commercial JCSG+ crystallization grid consisting of 0.1 M Bis-tris pH 5.5 and 1.6 M $(NH_4)_2SO_4$ (Quiagen). Drops were equilibrated against 500 μl. The best SIGN-R1 native crystal appears after 2 weeks with a maximum dimension of approximately 0.30 × 0.28 × 0.10 mm. Complexes of SIGN-R1 with dextran sulfate polysaccharide were obtained by incubation of a 4 mg/ml protein solution with 5 mM $CaCl_2$ and 3% dextran sulfate (Hampton research additive number 51). Best complex crystals appear after 3 weeks with maximum dimensions of approximately 0.20 × 0.18 × 0.10 mm. Complexes of the SIGN-R1 with sialic acid were obtained after overnight soaking of SIGN-R1 native crystals with precipitant solution supplemented with 10 mM sialic acid (SIGMA). All crystals were cryoprotected into a mixture of 3M Li_2SO_4 with crystallization conditions in a 1:1 volume proportion. Then, crystals were flash-cooled in liquid nitrogen and maintained at 100 K during data collection.

Crystallization of the Glycosylated Human Fc

Crystals were obtained by mixing 1 μl of Fc-Sial (9 mg/ml) with 3 μl of precipitant solution consisting of 0.1 M HEPES pH 7.0 and 0.1 M PEG 6000 under hanging drop vapor diffusion experiment at 18°C. The best Fc-Sial crystals appear after 2 weeks, reaching maximum dimensions of approximately 0.70 × 0.30 × 0.40 mm. Before data collection crystals were cryoprotected in a solution containing mother liquor and 25% glycerol. Then, crystals were flash-cooled in liquid nitrogen and maintained at 100 K during data collection.

X-Ray Data Collection and Structural Determination

X-ray data sets of CRD_SIGN-R1 native and ligand complexes were collected using a synchrotron radiation source at the ESRF (Grenoble). The native crystals data set was measured with an ADSC Quantum Q315r detector at beamline ID23-1. SIGN-R1:DexS data sets were measured with an ADSC Quantum 4 detector at beamline ID14-2. SIGN-R1:NeuAc data sets were measured with a MAR225 detector at beamline ID23-2. All data sets were processed using MOSFLM (Moras et al., 1992) and scaled using SCALA from the CCP4 package (CCP4, 1994). All SIGN-R1 crystals belong to monoclinic *C2* space group containing four independent molecules in the asymmetric unit. Data processing results are summarized in Table 1.

The native structure was determined by molecular replacement with MOLREP program from the CCP4 package (CCP4, 1994) using human DC-SIGN structure (PDB code ISL4) with 69% of identity, as initial model. Molecular replacement rotation and translation correlation coefficients were ranked and yielded four solutions well above the background; the final solution for R and S_{cor} were 39.7% and 57.3%, respectively.

X-ray data sets for sialylated Fc were measured with a Q315r ADSC CCD detector on ID14-4 beamline (ESRF, Grenoble). Crystals belong to the $P2_12_12_1$ orthorhombic space group containing two molecules in the asymmetric unit. Structural determination was done by molecular replacement using a monomer of the human IgG1 structure (PDB code IHZH), which shows 99% sequence identity for the Fc portion. Molecular replacement was performed with the MOLREP using a 3.5 Å cutoff limit for resolution. Four single and unambiguous solutions were obtained, with final correlation coefficients of 25% for R and 54% for $S_{cor.}$

In all cases, initial refinement and map calculations were carried out using CNS (Brünger et al., 1998). Bulk solvent correction was applied during the refinement. Water molecules were gradually added to peaks higher than 3σ in F_o-F_c maps with WATERPICK program routine of *CNS* program. Iterative cycles of refinement and manual model building were done. Model building was performed with Coot (Emsley and Cowtan, 2004) program. Further refinement using maximum likelihood methods was performed with the REFMAC5 from the CCP4 package (CCP4, 1994) and PHENIX (Adams et al., 2010) program. The final geometry of the structures was evaluated using the program PROCHECK (Laskowski et al., 1993). All the final models presented good stereochemistry parameters and *R* and R_{free} values (Table 1).

Docking Calculations

Two polysaccharides were docked at the SIGN-R1 secondary binding site: the capsular pneumococcal polysaccharide 14 (CPS14) and the polyribitol phosphate. The protein-ligand docking experiments were performed to test whether it was possible to find a compatible model with the experimental evidence of the repetitive Glucose-S/sulfate moieties observed in the crystallographic studies. To this end, we first docked the CPS14, one of the highest affinity capsular polysaccharide reported to bind to SIGN-R1 (Kang et al., 2004). The 3D structure of CPS14 was modeled in the sweet server (http://www.glycosciences.de/modeling/sweet2/doc/index.php), using the unit repetitive tetrasaccharide of the *S. pneumoniae* serotype 14 βGal(1,4)-βNAG(1,3)-βGal(1,4) βGlc(1,6)- βNAG as a template. Molecular docking was carried out using GOLD (Genetic Optimization for Ligand Docking) software (Verdonk et al., 2003), using the genetic algorithm (GA). This method allows a partial flexibility of protein and full flexibility of the ligand. For each of the

25 independent GA runs, a maximum number of 100,000 operations were performed on a set of five groups with a population size of 100 individuals. Default cut-off values of 2.5 Å (dH-X) for hydrogen bonds and 4.0 Å for Van Deer Waals distance were used. When the top three solutions attained rmsd values within 1.5 Å, GA docking was terminated. The rmsd values for the docking calculations are based on the rmsd matrix of the ranked solutions. We observed that the best-ranked solutions were always among the first ten GA runs, and the conformation of molecules based on the best fitness score was further analyzed. The Hex6 docking program (Ritchie et al., 2008) was also used to explore possible modes of interaction of SIGN-R1 with CPS14 models. This procedure performs a global rotational and translational space scan using Fourier transformations that rank the output according to surface complementarity and predicted electrostatic potentials. A list with the best complexes CPS14-SIGN-R1 was analyzed in a base of available biochemical data to filter out possible solutions. A similar disposition to that provided by GOLD was found for the polysaccharide using Hex6.

The 3D structure of (4)-ribitol phosphate was modeled using the Dundee PRODRG2 server (Schüttelkopf and van Aalten, 2004). Stereochemistry of the ligand was checked with the Mercury program (Macrae et al., 2008). Molecular docking was carried out using GOLD (Genetic Optimization for Ligand Docking) software (Verdonk et al., 2003) in a similar way to that used for CPS14. The cavity was defined from and to 5 Å around the 4 sulfates (S2–S5), giving freedom of movement to Lys197, Asn204, and Arg246 in side chain rotamers. The best-ranked solutions were always among the first 10 GA runs, and the conformation of molecules based on the best fitness score was further analyzed.

Molecular Dynamics Simulations

Simulations were based on the crystal structure of the human Fc fragment immunoglobulin reported in this paper. Long simulations were performed to investigate the dynamics of the sialic acid in positions 2–6 and 2–3. We used the crystallographic structure of 1MCO (Guddat et al., 1993) as a reference for the 2–3 conformation. The final glycosides molecules where prepared for the Glycam_06 (Kirschner et al., 2008) force field, whereas the AMBER ff99SB (Hornak et al., 2006) force field was used for the protein structure. Prepared structures were immersed in triclinic boxes of TIP3P water molecules (Jorgensen et al., 1993). Counter ions were also added to maintain electroneutrality. Before and after the addition of ions, two minimizations of 10,000 iterations were performed using a steepest descend and conjugated gradient method.

All minimizations and MD simulations were performed using the GROMACS 4 (Hess et al., 2008). Time steps of 2 fs were used for the integrations of Newton's equations of motion. The simulations have been carried out using periodic boundary conditions with the NPT (N, total number of atoms; P, pressure; T, temperature) ensemble. Electrostatic interactions were evaluated using the particle-mesh Ewald (PME) method (Darden et al., 1993) with Van der Waals interactions truncated at 14 Å. The systems were then heated and equilibrated in two steps: (1) 300 ps of MD with restricted position of all atoms of the glycoprotein and heating whole system from 50 K to 298 K, and (2) 150 ps of MD with restricted position of the backbone atoms. The equilibrated structures were the starting points for 200 ns MD simulations at constant temperature (298 K) and pressure (1 atm). Bond lengths were constrained using the LINCS algorithm, and water geometries constrained by SETTLE. Analyses were performed using the GROMACS 4 suite of programs. Demonstration of system geometries and interactions were done using CHIMERA.

ACCESSION NUMBERS

The Protein Data Bank accession numbers for the atomic coordinates codes reported in this paper are 3ZHG(SIGN-R1), 4C9F (SIGN-R1:sulfodextran complex), 4CAJ (SIGN-R1:sialic acid complex), and 4CDH (α-2,6 sialylated antibody FC).

SUPPLEMENTAL INFORMATION

Supplemental Information includes six figures and two movies and can be found with this article online at http://dx.doi.org/10.1016/j.str.2014.09.001.

AUTHOR CONTRIBUTIONS

N.S-M. performed crystallography and analyzed the crystallographic data, S.G.B. analyzed the crystallographic data, C.G.P. cloned genes and purified proteins, E.R. and P.C. performed the computational analysis, C.G.P. executed binding experiments, C.G.P. and J.A.H. analyzed the data, and C.G.P. and J.A.H. conceived experiments and wrote the paper.

ACKNOWLEDGMENTS

We are deeply grateful for the help and advice from the late Ralph Steinman. We thank Robert M. Anthony and Jeffrey Ravetch for providing the α-2,6 sialylated antibody Fc portion and for critical reading of the manuscript. This work was supported by grants from the Spanish Ministry of Economy and Competitiveness (BFU2011-25326; to J.A.H.) and the biomedicine program of government of autonomous community of Madrid (S2010/BMD-2457; to J.A.H.) and a faculty research grant of Yonsei University College of Medicine for 2013 (6-2013-0062; to C.G.P.).

Received: May 23, 2014
Revised: September 2, 2014
Accepted: September 3, 2014
Published: October 23, 2014

REFERENCES

Abeyta, M., Hardy, G.G., and Yother, J. (2003). Genetic alteration of capsule type but not PspA type affects accessibility of surface-bound complement and surface antigens of Streptococcus pneumoniae. Infect. Immun. *71*, 218–225.

Adams, P.D., Afonine, P.V., Bunkóczi, G., Chen, V.B., Davis, I.W., Echols, N., Headd, J.J., Hung, L.W., Kapral, G.J., Grosse-Kunstleve, R.W., et al. (2010). PHENIX: a comprehensive Python-based system for macromolecular structure solution. Acta Crystallogr. D Biol. Crystallogr. *66*, 213–221.

Anthony, R.M., and Ravetch, J.V. (2010). A novel role for the IgG Fc glycan: the anti-inflammatory activity of sialylated IgG Fcs. J. Clin. Immunol. *30* (*Suppl 1*), S9–S14.

Anthony, R.M., Wermeling, F., Karlsson, M.C.I., and Ravetch, J.V. (2008). Identification of a receptor required for the anti-inflammatory activity of IVIG. Proc. Natl. Acad. Sci. USA *105*, 19571–19578.

Anthony, R.M., Kobayashi, T., Wermeling, F., and Ravetch, J.V. (2011). Intravenous gammaglobulin suppresses inflammation through a novel T(H)2 pathway. Nature *475*, 110–113.

Brown, J.S., Hussell, T., Gilliland, S.M., Holden, D.W., Paton, J.C., Ehrenstein, M.R., Walport, M.J., and Botto, M. (2002). The classical pathway is the dominant complement pathway required for innate immunity to Streptococcus pneumoniae infection in mice. Proc. Natl. Acad. Sci. USA *99*, 16969–16974.

Brünger, A.T., Adams, P.D., Clore, G.M., DeLano, W.L., Gros, P., Grosse-Kunstleve, R.W., Jiang, J.S., Kuszewski, J., Nilges, M., Pannu, N.S., et al. (1998). Crystallography & NMR system: A new software suite for macromolecular structure determination. Acta Crystallogr. D Biol. Crystallogr. *54*, 905–921.

Caminschi, I., Corbett, A.J., Zahra, C., Lahoud, M., Lucas, K.M., Sofi, M., Vremec, D., Gramberg, T., Pöhlmann, S., Curtis, J., et al. (2006). Functional comparison of mouse CIRE/mouse DC-SIGN and human DC-SIGN. Int. Immunol. *18*, 741–753.

CCP4 (Collaborative Computational Project, Number 4) (1994). The CCP4 suite: programs for protein crystallography. Acta Crystallogr. D Biol. Crystallogr. *50*, 760–763.

Chehimi, J., Luo, Q., Azzoni, L., Shawver, L., Ngoubilly, N., June, R., Jerandi, G., Farabaugh, M., and Montaner, L.J. (2003). HIV-1 transmission and cytokine-induced expression of DC-SIGN in human monocyte-derived macrophages. J. Leukoc. Biol. *74*, 757–763.

Cheong, C., Matos, I., Choi, J.H., Dandamudi, D.B., Shrestha, E., Longhi, M.P., Jeffrey, K.L., Anthony, R.M., Kluger, C., Nchinda, G., et al. (2010). Microbial

stimulation fully differentiates monocytes to DC-SIGN/CD209(+) dendritic cells for immune T cell areas. Cell *143*, 416–429.

Colino, J., and Snapper, C.M. (2007). Dendritic cell-derived exosomes express a Streptococcus pneumoniae capsular polysaccharide type 14 cross-reactive antigen that induces protective immunoglobulin responses against pneumococcal infection in mice. Infect. Immun. *75*, 220–230.

Crispin, M., Yu, X., and Bowden, T.A. (2013). Crystal structure of sialylated IgG Fc: implications for the mechanism of intravenous immunoglobulin therapy. Proc. Natl. Acad. Sci. USA *110*, E3544–E3546.

Curtis, B.M., Scharnowske, S., and Watson, A.J. (1992). Sequence and expression of a membrane-associated C-type lectin that exhibits CD4-independent binding of human immunodeficiency virus envelope glycoprotein gp120. Proc. Natl. Acad. Sci. USA *89*, 8356–8360.

Darden, T., York, D., and P, L. (1993). Particle mesh Ewald. An N-log(N) method for Ewald sums in large systems. J. Chem. Phys. *98*, 10089–10092.

Emsley, P., and Cowtan, K. (2004). Coot: model-building tools for molecular graphics. Acta Crystallogr. D Biol. Crystallogr. *60*, 2126–2132.

Feinberg, H., Castelli, R., Drickamer, K., Seeberger, P.H., and Weis, W.I. (2007). Multiple modes of binding enhance the affinity of DC-SIGN for high mannose N-linked glycans found on viral glycoproteins. J. Biol. Chem. *282*, 4202–4209.

Gaboriaud, C., Juanhuix, J., Gruez, A., Lacroix, M., Darnault, C., Pignol, D., Verger, D., Fontecilla-Camps, J.C., and Arlaud, G.J. (2003). The crystal structure of the globular head of complement protein C1q provides a basis for its versatile recognition properties. J. Biol. Chem. *278*, 46974–46982.

Galustian, C., Park, C.G., Chai, W., Kiso, M., Bruening, S.A., Kang, Y.-S., Steinman, R.M., and Feizi, T. (2004). High and low affinity carbohydrate ligands revealed for murine SIGN-R1 by carbohydrate array and cell binding approaches, and differing specificities for SIGN-R3 and langerin. Int. Immunol. *16*, 853–866.

Geijtenbeek, T.B., Torensma, R., van Vliet, S.J., van Duijnhoven, G.C., Adema, G.J., van Kooyk, Y., and Figdor, C.G. (2000). Identification of DC-SIGN, a novel dendritic cell-specific ICAM-3 receptor that supports primary immune responses. Cell *100*, 575–585.

Geijtenbeek, T.B., Groot, P.C., Nolte, M.A., van Vliet, S.J., Gangaram-Panday, S.T., van Duijnhoven, G.C., Kraal, G., van Oosterhout, A.J., and van Kooyk, Y. (2002). Marginal zone macrophages express a murine homologue of DC-SIGN that captures blood-borne antigens in vivo. Blood *100*, 2908–2916.

Gordon, S. (2002). Pattern recognition receptors: doubling up for the innate immune response. Cell *111*, 927–930.

Granelli-Piperno, A., Pritsker, A., Pack, M., Shimeliovich, I., Arrighi, J.F., Park, C.G., Trumpfheller, C., Piguet, V., Moran, T.M., and Steinman, R.M. (2005). Dendritic cell-specific intercellular adhesion molecule 3-grabbing nonintegrin/CD209 is abundant on macrophages in the normal human lymph node and is not required for dendritic cell stimulation of the mixed leukocyte reaction. J. Immunol. *175*, 4265–4273.

Guddat, L.W., Herron, J.N., and Edmundson, A.B. (1993). Three-dimensional structure of a human immunoglobulin with a hinge deletion. Proc. Natl. Acad. Sci. USA *90*, 4271–4275.

Guo, Y., Feinberg, H., Conroy, E., Mitchell, D.A., Alvarez, R., Blixt, O., Taylor, M.E., Weis, W.I., and Drickamer, K. (2004). Structural basis for distinct ligand-binding and targeting properties of the receptors DC-SIGN and DC-SIGNR. Nat. Struct. Mol. Biol. *11*, 591–598.

Hess, B., Kutzner, C., van der Spoel, D., and Lindahl, E. (2008). GROMACS 4: algorithms for highly efficient, load-balanced, and scalable molecular simulation. J. Chem. Theory Comput. *4*, 435–447.

Hornak, V., Abel, R., Okur, A., Strockbine, B., Roitberg, A., and Simmerling, C. (2006). Comparison of multiple Amber force fields and development of improved protein backbone parameters. Proteins *65*, 712–725.

Jorgensen, W.L., Chandrasekhar, J., Madura, J.D., Impey, R.D., and Klein, M.L. (1993). Comparison of simple potential functions for simulating liquid water. J. Chem. Phys. *79*, 926–935.

Kaneko, Y., Nimmerjahn, F., and Ravetch, J.V. (2006). Anti-inflammatory activity of immunoglobulin G resulting from Fc sialylation. Science *313*, 670–673.

Kang, Y.-S., Yamazaki, S., Iyoda, T., Pack, M., Bruening, S.A., Kim, J.Y., Takahara, K., Inaba, K., Steinman, R.M., and Park, C.G. (2003). SIGN-R1, a novel C-type lectin expressed by marginal zone macrophages in spleen, mediates uptake of the polysaccharide dextran. Int. Immunol. *15*, 177–186.

Kang, Y.-S., Kim, J.Y., Bruening, S.A., Pack, M., Charalambous, A., Pritsker, A., Moran, T.M., Loeffler, J.M., Steinman, R.M., and Park, C.G. (2004). The C-type lectin SIGN-R1 mediates uptake of the capsular polysaccharide of Streptococcus pneumoniae in the marginal zone of mouse spleen. Proc. Natl. Acad. Sci. USA *101*, 215–220.

Kang, Y.-S., Do, Y., Lee, H.-K., Park, S.H., Cheong, C., Lynch, R.M., Loeffler, J.M., Steinman, R.M., and Park, C.G. (2006). A dominant complement fixation pathway for pneumococcal polysaccharides initiated by SIGN-R1 interacting with C1q. Cell *125*, 47–58.

Kirschner, K.N., Yongye, A.B., Tschampel, S.M., González-Outeiriño, J., Daniels, C.R., Foley, B.L., and Woods, R.J. (2008). GLYCAM06: a generalizable biomolecular force field. Carbohydrates. J. Comput. Chem. *29*, 622–655.

Koesling, J., Lucas, B., Develioglou, L., Aebischer, T., and Meyer, T.F. (2001). Vaccination of mice with live recombinant Salmonella typhimurium aroA against H. pylori: parameters associated with prophylactic and therapeutic vaccine efficacy. Vaccine *20*, 413–420.

Lanoue, A., Clatworthy, M.R., Smith, P., Green, S., Townsend, M.J., Jolin, H.E., Smith, K.G.C., Fallon, P.G., and McKenzie, A.N.J. (2004). SIGN-R1 contributes to protection against lethal pneumococcal infection in mice. J. Exp. Med. *200*, 1383–1393.

Laskowski, R.A., Moss, D.S., and Thornton, J.M. (1993). Main-chain bond lengths and bond angles in protein structures. J. Mol. Biol. *231*, 1049–1067.

Macrae, C.F., Bruno, I.J., Chisholm, J.A., Edgington, P.R., McCabe, P., Pidcock, E., Rodriguez-Monge, L., Taylor, R., van de Streek, J., and Wood, P.A. (2008). Mercury CSD 2.0 - new features for the visualization and investigation of crystal structures. J. Appl. Cryst. *41*, 466–470.

Meyer-Wentrup, F., Cambi, A., Adema, G.J., and Figdor, C.G. (2005). "Sweet talk": closing in on C type lectin signaling. Immunity *22*, 399–400.

Mizuochi, T., Yonemasu, K., Yamashita, K., and Kobata, A. (1978). The asparagine-linked sugar chains of subcomponent C1q of the first component of human complement. J. Biol. Chem. *253*, 7404–7409.

Moras, D., Podjarny, A.D., and Thierry, J.C., eds. (1992). Crystallographic Computing 5: From Chemistry to Biology (Oxford, UK: Oxford University Press), pp. 39–50.

Nagaoka, K., Takahara, K., Tanaka, K., Yoshida, H., Steinman, R.M., Saitoh, S., Akashi-Takamura, S., Miyake, K., Kang, Y.S., Park, C.G., and Inaba, K. (2005). Association of SIGNR1 with TLR4-MD-2 enhances signal transduction by recognition of LPS in gram-negative bacteria. Int. Immunol. *17*, 827–836.

Nagaoka, K., Takahara, K., Minamino, K., Takeda, T., Yoshida, Y., and Inaba, K. (2010). Expression of C-type lectin, SIGNR3, on subsets of dendritic cells, macrophages, and monocytes. J. Leukoc. Biol. *88*, 913–924.

Park, C.G., Takahara, K., Umemoto, E., Yashima, Y., Matsubara, K., Matsuda, Y., Clausen, B.E., Inaba, K., and Steinman, R.M. (2001). Five mouse homologues of the human dendritic cell C-type lectin, DC-SIGN. Int. Immunol. *13*, 1283–1290.

Park, S.H., Cheong, C., Idoyaga, J., Kim, J.Y., Choi, J.H., Do, Y., Lee, H., Jo, J.H., Oh, Y.S., Im, W., et al. (2008). Generation and application of new rat monoclonal antibodies against synthetic FLAG and OLLAS tags for improved immunodetection. J. Immunol. Methods *331*, 27–38.

Powlesland, A.S., Ward, E.M., Sadhu, S.K., Guo, Y., Taylor, M.E., and Drickamer, K. (2006). Widely divergent biochemical properties of the complete set of mouse DC-SIGN-related proteins. J. Biol. Chem. *281*, 20440–20449.

Prabagar, M.G., Do, Y., Ryu, S., Park, J.Y., Choi, H.J., Choi, W.S., Yun, T.J., Moon, J., Choi, I.S., Ko, K., et al. (2013). SIGN-R1, a C-type lectin, enhances apoptotic cell clearance through the complement deposition pathway by interacting with C1q in the spleen. Cell Death Differ. *20*, 535–545.

Ritchie, D.W., Kozakov, D., and Vajda, S. (2008). Accelerating and focusing protein-protein docking correlations using multi-dimensional rotational FFT generating functions. Bioinformatics *24*, 1865–1873.

Schüttelkopf, A.W., and van Aalten, D.M. (2004). PRODRG: a tool for high-throughput crystallography of protein-ligand complexes. Acta Crystallogr. D Biol. Crystallogr. *60*, 1355–1363.

Silva-Martin, N., Schauer, J.D., Park, C.G., and Hermoso, J.A. (2009). Crystallization and preliminary X-ray diffraction studies of the carbohydrate-recognition domain of SIGN-R1, a receptor for microbial polysaccharides and sialylated antibody on splenic marginal zone macrophages. Acta Crystallogr. Sect. F Struct. Biol. Cryst. Commun. *65*, 1264–1266.

Sondermann, P., Pincetic, A., Maamary, J., Lammens, K., and Ravetch, J.V. (2013a). General mechanism for modulating immunoglobulin effector function. Proc. Natl. Acad. Sci. USA *110*, 9868–9872.

Sondermann, P., Pincetic, A., Maamary, J., Lammens, K., and Ravetch, J.V. (2013b). Reply to Crispin et al.: Molecular model that accounts for the biological and physical properties of sialylated Fc. Proc. Natl. Acad. Sci. USA *110*, E3547.

Takahara, K., Yashima, Y., Omatsu, Y., Yoshida, H., Kimura, Y., Kang, Y.S., Steinman, R.M., Park, C.G., and Inaba, K. (2004). Functional comparison of the mouse DC-SIGN, SIGNR1, SIGNR3 and Langerin, C-type lectins. Int. Immunol. *16*, 819–829.

Varchetta, S., Lusso, P., Hudspeth, K., Mikulak, J., Mele, D., Paolucci, S., Cimbro, R., Malnati, M., Riva, A., Maserati, R., et al. (2013). Sialic acid-binding Ig-like lectin-7 interacts with HIV-1 gp120 and facilitates infection of CD4pos T cells and macrophages. Retrovirology *10*, 154.

Verdonk, M.L., Cole, J.C., Hartshorn, M.J., Murray, C.W., and Taylor, R.D. (2003). Improved protein-ligand docking using GOLD. Proteins *52*, 609–623.

Weidenmaier, C., and Peschel, A. (2008). Teichoic acids and related cell-wall glycopolymers in Gram-positive physiology and host interactions. Nat. Rev. Microbiol. *6*, 276–287.

Zelensky, A.N., and Gready, J.E. (2003). Comparative analysis of structural properties of the C-type-lectin-like domain (CTLD). Proteins *52*, 466–477.

